Contents lists available at ScienceDirect

Physics Letters B

www.elsevier.com/locate/physletb

Transverse extension of partons in the proton probed in the sea-quark range by measuring the DVCS cross section

The COMPASS Collaboration

ABSTRACT

We report on the first measurement of exclusive single-photon muoproduction on the proton by COMPASS using $160\,\text{GeV}/c$ polarised μ^+ and μ^- beams of the CERN SPS impinging on a liquid hydrogen target. We determine the dependence of the average of the measured μ^+ and μ^- cross sections for deeply virtual Compton scattering on the squared four-momentum transfer t from the initial to the final proton. The slope B of the t-dependence is fitted with a single exponential function, which yields $B = (4.3 \pm 0.6_\text{stat} \, {}^{+\,0.1}_{-\,0.3}\big|_\text{sys}) \, (\text{GeV}/c)^{-2}$. This result can be converted into a transverse extension of partons in the proton, $\sqrt{\langle r_\perp^2 \rangle} = (0.58 \pm 0.04_\text{stat} \, {}^{+\,0.01}_{-\,0.02}\big|_\text{sys} \pm 0.04_\text{model}) \, \text{fm}$. For this measurement, the average virtuality of the photon mediating the interaction is $\langle Q^2 \rangle = 1.8 \, (\text{GeV}/c)^2$ and the average value of the Bjorken variable is $\langle x_\text{Bj} \rangle = 0.056$.

1. Introduction

The structure of the proton has been studied over half a century, still its understanding constitutes one of the very important challenges that physics is facing today. Quantum Chromodynamics (QCD), the theory of strong interaction that governs the dynamics of quarks and gluons as constituents of the proton, is presently not analytically solvable. Lepton-proton scattering experiments have been proven to be very powerful tools to unravel the internal dynamics of the proton: (i) elastic scattering allows access to charge and current distributions in the proton by measuring electromagnetic form factors; (ii) deep-inelastic scattering (DIS) provides important information on the density distributions as a function of longitudinal momentum for quarks and gluons in the proton, encoded in universal parton distribution functions.

Deeply virtual Compton scattering (DVCS), $\gamma^* p \to \gamma p$, is the production of a single real photon γ through the absorption of a virtual photon γ^* by a proton p. This process combines features of the elastic process and those of the inelastic processes. Using the concept of generalized parton distributions (GPDs) [1–5], it was shown [6–9] that in a certain kinematic domain DVCS allows access to correlations between transverse-position and longitudinal-momentum distributions of the partons in the proton. Here, longitudinal and transverse refer to the direction of motion of the initial proton facing the virtual photon. The measurement of DVCS probes the transverse extension of the parton density in the proton over the experimentally accessible region of longitudinal momentum of

the active parton. Exploring the interplay between longitudinal and transverse partonic degrees of freedom by DVCS is often referred to as "proton tomography". The DVCS process is studied through exclusive single-photon production in lepton-proton scattering. The experimental results obtained so far are discussed in a recent review [10].

In this Letter, we present the result on a measurement of the DVCS cross section obtained by studying exclusive single-photon production in muon-proton scattering, $\mu p \to \mu' p' \gamma$. Following Refs. [6,7,11–13], the slope B of the measured exponential t-dependence of the differential DVCS cross section can approximately be converted into the average squared transverse extension of partons in the proton as probed by DVCS,

$$\langle r_\perp^2 (x_\text{Bj}) \rangle \approx 2 \langle B(x_\text{Bj}) \rangle \hbar^2, \qquad (1)$$

which is measured at the average value of x_Bj accessed by COMPASS. The approximation used above is discussed in Sec. 5. In the following we refer to $\sqrt{\langle r_\perp^2 \rangle}$ as transverse extension of partons. Here, t is the squared four-momentum transferred to the target proton, $x_\text{Bj} = Q^2/(2M\nu)$ the Bjorken variable, $Q^2 = -(k_\mu - k_{\mu'})^2$, and $\nu = (k_\mu^0 - k_{\mu'}^0)$ the energy of the virtual photon in the target rest frame, with k_μ and $k_{\mu'}$ denoting the four-momenta of the incoming and scattered muon, respectively, and M the proton mass. The quantity $r_\perp$ is the transverse distance between the active quark and the centre of momentum of the spectator quarks
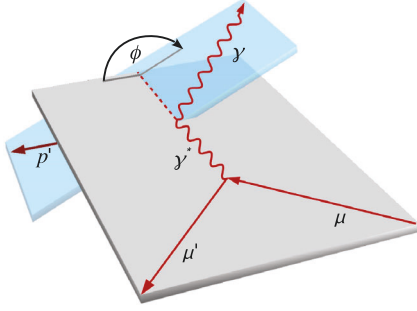
Fig. 1. Definition of ϕ, the azimuthal angle between the lepton-scattering and photon-production planes.

and is hence used in this Letter to represent the transverse extension of partons in the proton.

Using boldface letters for particle three-momenta, defining $\mathbf{q} = \mathbf{k}_\mu - \mathbf{k}_{\mu'}$, denoting by $\mathbf{p}_\gamma$ the momentum of the real photon, and calculating the azimuthal angle between the lepton-scattering and photon-production planes (see also Fig. 1) as

$$\phi = \frac{(\mathbf{q} \times \mathbf{k}_\mu) \cdot \mathbf{p}_\gamma}{|(\mathbf{q} \times \mathbf{k}_\mu) \cdot \mathbf{p}_\gamma|} \arccos\left(\frac{(\mathbf{q} \times \mathbf{k}_\mu) \cdot (\mathbf{q} \times \mathbf{p}_\gamma)}{|\mathbf{q} \times \mathbf{k}_\mu||\mathbf{q} \times \mathbf{p}_\gamma|}\right), \quad (2)$$

the cross section of muon-induced single-photon production is written as

$$d\sigma := \frac{d^4\sigma^{\mu p}}{dQ^2 d\nu dt d\phi}. \quad (3)$$

This cross section was measured separately using either a μ^+ or a μ^- beam of 160 GeV/c average momentum, which was provided by the M2 beamline of the CERN SPS. The natural polarisation of the muon beam originates from the parity-violating decay-in-flight of the parent mesons, which implies opposite signs of the polarisation for the used μ^+ and μ^- beams. For both beams, the absolute value of the average beam polarisation is about 0.8 with an uncertainty of about 0.04. Denoting charge and helicity of an incident muon by $\pm$ and $\leftrightarrows$, respectively, the sum of the cross sections for μ^+ and μ^- beams reads:

$$2\,d\sigma \equiv d\sigma^{\overset{+}{\leftarrow}} + d\sigma^{\overset{-}{\rightarrow}} = 2(d\sigma^{BH} + d\sigma^{DVCS} - |P_\mu|d\sigma^I). \quad (4)$$

Here, P_μ denotes the polarisation of the muon beam. The single-photon final state in lepton-nucleon scattering can also originate from the Bethe-Heitler (BH) process, i.e. photon emission from either the incoming or outgoing lepton. Hence the DVCS and BH processes interfere, so that the above sum of μ^+ and μ^- cross sections comprises not only the contributions $d\sigma^{DVCS}$ and $d\sigma^{BH}$ but also that from the interference term denoted by $d\sigma^I$.

At sufficiently large values of Q^2 and small values of $|t|$, the azimuthal dependences of the DVCS cross section and of the interference term including twist-3 contributions read as follows [14]:

$$d\sigma^{DVCS} \propto \frac{1}{y^2 Q^2}(c_0^{DVCS} + c_1^{DVCS}\cos\phi + c_2^{DVCS}\cos 2\phi),$$

$$d\sigma^I \propto \frac{1}{x_{Bj}y^3 t P_1(\phi)P_2(\phi)}(s_1^I \sin\phi + s_2^I \sin 2\phi). \quad (5)$$

Here, $P_1(\phi)$ and $P_2(\phi)$ are the BH lepton propagators, y is the fractional energy of the virtual photon, and c_i^{DVCS} and s_i^I are related to certain combinations of Compton Form Factors (CFFs) [14]. The latter are convolutions of GPDs with functions describing the Compton interaction at the parton level. At leading order in the

strong coupling constant α_S and using the leading-twist approximation, in Eq. (5) only the terms containing c_0^{DVCS} and s_1^I remain. In terms of Compton helicity amplitudes, this corresponds to the dominance of the amplitude that describes the transition from a transversely polarized virtual photon to a transversely polarised real photon.

After subtracting the cross section of the BH process, $d\sigma^{BH}$, from Eq. (4) and integrating the remainder over ϕ, all azimuth-dependent terms disappear and only the dominant contribution from transversely polarized virtual photons to the DVCS cross section remains. It is indicated by the subscript T:

$$\frac{d^3\sigma_T^{\mu p}}{dQ^2 d\nu dt} = \int_{-\pi}^{\pi} d\phi \, (d\sigma - d\sigma^{BH}) \propto c_0^{DVCS}. \quad (6)$$

This cross section is converted into the cross section for virtual-photon scattering using the flux $\Gamma(Q^2, \nu, E_\mu)$ for transverse virtual photons,

$$\frac{d\sigma^{\gamma^* p}}{dt} = \frac{1}{\Gamma(Q^2, \nu, E_\mu)}\frac{d^3\sigma_T^{\mu p}}{dQ^2 d\nu dt}, \quad (7)$$

with

$$\Gamma(Q^2, \nu, E_\mu) = \frac{\alpha_{em}(1 - x_{Bj})}{2\pi Q^2 y E_\mu}\left[y^2\left(1 - \frac{2m_\mu^2}{Q^2}\right) + \frac{2}{1 + Q^2/\nu^2}\left(1 - y - \frac{Q^2}{4E_\mu^2}\right)\right], \quad (8)$$

for which the Hand convention [15] is used. Here, m_μ and E_μ denote the mass and energy of the incoming muon, respectively, and α_{em} the electromagnetic fine-structure constant.

2. Experimental set-up

The data used for this analysis were recorded during four weeks in 2012 using the COMPASS set-up. The muon beam was centred onto a 2.5 m long liquid-hydrogen target surrounded by two concentric cylinders consisting of slats of scintillating counters, which detected recoiling protons by the time-of-flight (ToF) technique. The first electromagnetic calorimeter (ECAL0) was placed directly downstream of the target to detect photons emitted at large polar scattering angles. Particles emitted through its central opening into the forward direction were measured using the open-field two-stage magnetic spectrometer. Each spectrometer stage comprised an electromagnetic calorimeter (ECAL1 or ECAL2), a hadron calorimeter, a muon filter for muon identification, and a variety of tracking detectors. A detailed description of the spectrometer can be found in Refs. [16–18]. The period of data taking was divided into several subperiods. After each subperiod, charge and polarisation of the muon beam were swapped simultaneously. The total integrated luminosity is 18.9 pb^{-1} for the μ^+ beam with negative polarisation and 23.5 pb^{-1} for the μ^- beam with positive polarisation.

3. Data analysis

The selected events are required to have at least one reconstructed vertex inside the liquid-hydrogen target associated with an incoming muon, a single outgoing particle of the same charge, a recoil proton candidate, and exactly one "neutral cluster" detected above 4 GeV, 5 GeV or 10 GeV in ECAL0, ECAL1, or ECAL2 respectively. Here, neutral cluster specifies a cluster not associated to a charged particle. For ECAL0 any cluster is considered as neutral, as
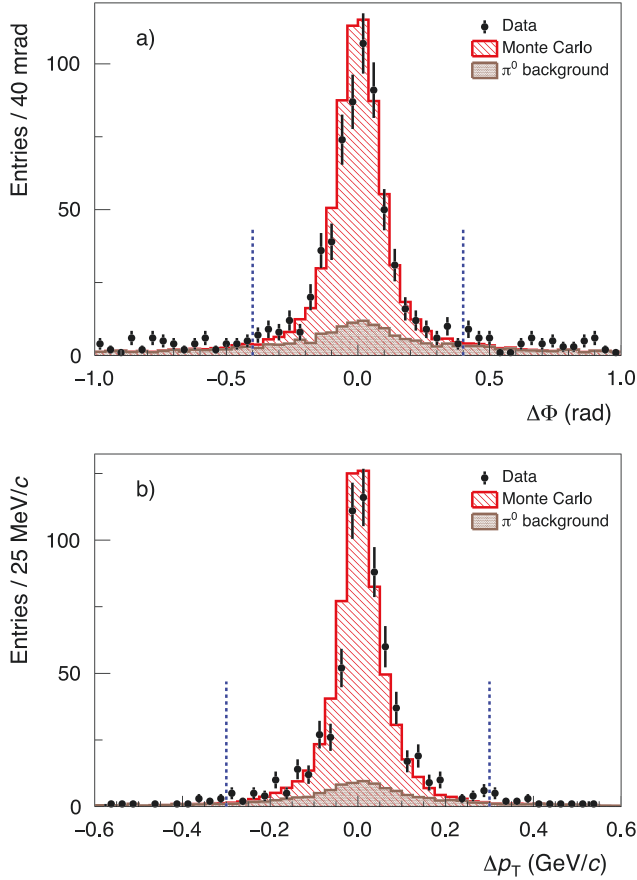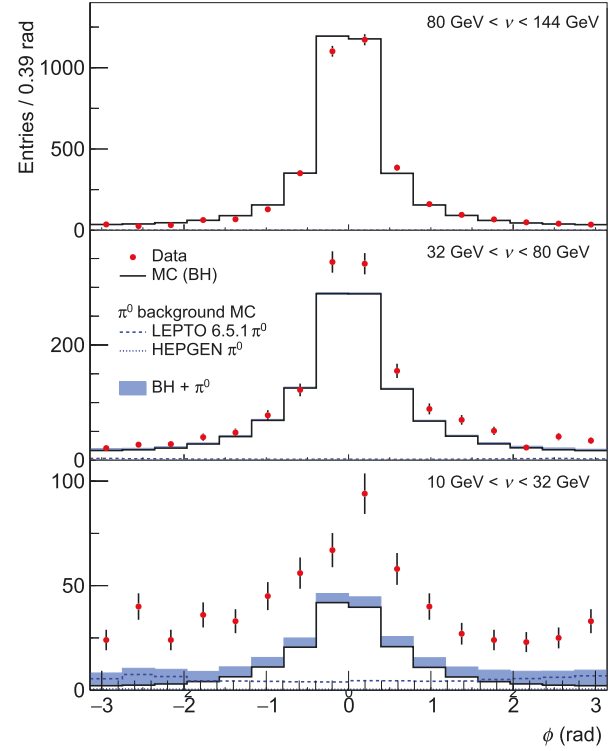
Fig. 2. Distribution of the difference between predicted and reconstructed values of (a) the azimuthal angle and (b) the transverse momentum of the recoiling proton candidates for $1\,(\mathrm{GeV}/c)^2 < Q^2 < 5\,(\mathrm{GeV}/c)^2$, $0.08\,(\mathrm{GeV}/c)^2 < |t| < 0.64\,(\mathrm{GeV}/c)^2$ and $10\,\mathrm{GeV} < \nu < 32\,\mathrm{GeV}$. The dashed blue vertical lines enclose the region accepted for analysis. Here, Monte Carlo also includes π^0 background.

Fig. 3. Number of reconstructed single-photon events as a function of ϕ in three regions of ν for $1\,(\mathrm{GeV}/c)^2 < Q^2 < 5\,(\mathrm{GeV}/c)^2$ and $0.08\,(\mathrm{GeV}/c)^2 < |t| < 0.64\,(\mathrm{GeV}/c)^2$. Error bars represent statistical uncertainties. Additionally shown are the sum of a Monte Carlo simulation of the BH process and the two components of the π^0 contamination described in the text. Note that the yield of the HEPGEN π^0 contribution is very small and at most 0.01, 0.2 or 0.6 entries per ϕ-bin in the panels from top to bottom, respectively. The data in this figure are not yet corrected for π^0 background.

there are no tracking detectors in front. An outgoing charged particle that traverses more than 15 radiation lengths is considered to be a muon. The spectrometer information on incoming and scattered muons, as well as on position and energy measured for the neutral cluster, is used together with measured information from the time-of-flight system of the target-recoil detector. For a given event, the kinematics of all recoil proton candidates are compared with the corresponding predictions that are obtained using spectrometer information only.

Exemplary results of this comparison are displayed in Fig. 2 using two variables that characterize the kinematics of the recoiling target particle. Fig. 2(a) shows the difference between the measured and the predicted azimuthal angle, $\Delta\Phi$, and Fig. 2(b) the difference between the measured and the predicted transverse momentum, Δp_T. Here, Φ and p_T are given in the laboratory system.

Fig. 2 shows additionally a comparison between the data and the sum of Monte Carlo yields that includes all single-photon production mechanisms, i.e. BH, DVCS and their interference, as well as the π^0 background estimates. The Monte Carlo simulations for all these mechanisms are based on the HEPGEN generator [19,20]. The adopted DVCS amplitude follows the model of Refs. [21,22], which was originally proposed to describe the DVCS data measured at very small x_Bj at HERA, with modifications required for COMPASS (see Refs. [19,23] and references therein). For the BH amplitude and the interference term, the formalism of Ref. [14] is used replacing the approximate expressions for the lepton propagators P1 and P2 by the exact formulae that take into account the

non-zero mass of the lepton. The HEPGEN simulations are normalized to the total integrated luminosity of the data. The simulations are also used for the calculation of the spectrometer acceptance.

In order to identify background events originating from π^0 production, where one photon of the π^0 decay is detected in an electromagnetic calorimeter but falls short of the above given threshold, the single-photon candidate is combined with every neutral cluster below threshold. The event is excluded if a π^0 with $|m_{\gamma\gamma} - m_{\pi^0}^{PDG}| < 20\,\mathrm{MeV}/c^2$ can be reconstructed. This corresponds to about 1.5 standard deviations of the mass resolution. The number of excluded events is used below to normalise the π^0 Monte Carlo simulation.

Background originating from π^0 production, where one photon of the π^0 decay remains undetected, is estimated using a Monte Carlo simulation that is normalised to the aforementioned excluded fraction of π^0 events. This simulation, which is denoted as π^0 background in Fig. 2, is the sum of two components. First, the HEPGEN generator uses the parameterisation of Ref. [24] for the cross section of the exclusive reaction $\mu p \to \mu p \pi^0$. Secondly, the LEPTO 6.5.1 generator with the COMPASS high-p_T tuning [25] is used to simulate the tail of non-exclusive π^0 production, which is accepted by our experimental selections. Comparing the two components to the data allows the determination of their relative normalisation.

After the application of the above described selection criteria a kinematic fit is performed, which is constrained by requiring a single-photon final state in order to obtain the best possible determination of all kinematic parameters in a given event. Fig. 3 shows the number of selected single-photon events as a function of ϕ for
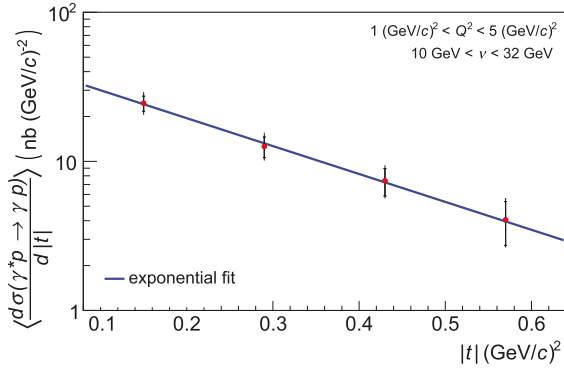
Fig. 4. Differential DVCS cross section as a function of $|t|$. The mean value of the cross section is shown at the centre of each of the four $|t|$-bins. The blue curve is the result of a binned maximum likelihood fit of an exponential function to the data. This fit integrates the exponential model over the respective t-bins and does not use their central values, which are used for illustration only. The probability to observe a similar or better agreement of the data with the blue curve is approximately 7%. Here and in the next figure, inner error bars represent statistical uncertainties and outer error bars the quadratic sum of statistical and systematic uncertainties.

Table 1
Values of the extracted DVCS cross section: The quantity $\langle \frac{d\sigma}{d|t|} \rangle$ denotes the average of the measured differential μ^+ and μ^- DVCS cross sections in the indicated $|t|$-bin. Apart from the integration over t, the cross section is integrated over Q^2 and ν and divided by the product of the respective bin widths, as indicated in Fig. 4. In addition, the mean values for Q^2 and ν are given for each of the four bins. These mean values are weighted averages with the weight being the virtual-photon proton cross section.

$\frac{|t|-\text{bin}}{(\text{GeV}/c)^2}$	$\frac{\langle \frac{d\sigma}{d|t|} \rangle}{\text{nb}(\text{GeV}/c)^{-2}}$	$\frac{\langle Q^2 \rangle}{(\text{GeV}/c)^2}$	$\frac{\langle \nu \rangle}{\text{GeV}}$
[0.08, 0.22]	$24.5 \pm 2.8_{\text{stat}} {}^{+3.7}_{-2.9}\big|_{\text{sys}}$	1.79	19.5
[0.22, 0.36]	$12.6 \pm 2.0_{\text{stat}} {}^{+2.2}_{-1.5}\big|_{\text{sys}}$	1.77	18.8
[0.36, 0.50]	$7.4 \pm 1.6_{\text{stat}} {}^{+1.3}_{-0.9}\big|_{\text{sys}}$	1.91	18.6
[0.50, 0.64]	$4.1 \pm 1.3_{\text{stat}} {}^{+1.0}_{-0.5}\big|_{\text{sys}}$	1.77	20.1

three different regions in the virtual-photon energy ν. The data are compared to the sum of a Monte Carlo simulation of the BH process only, which is normalised to the total integrated luminosity of the data, and the estimated π^0 contamination. For large values of ν, the data agree reasonably well with the expectation that only the BH process contributes. For intermediate and small values of ν, sizable contributions from the DVCS process and the BH-DVCS interference are observed.

From here on, the analysis is performed in the region of small ν using a three-dimensional equidistant grid with four bins in $|t|$ from 0.08 $(\text{GeV}/c)^2$ to 0.64 $(\text{GeV}/c)^2$, 11 bins in ν from 10 GeV to 32 GeV, and four bins in Q^2 from 1 $(\text{GeV}/c)^2$ to 5 $(\text{GeV}/c)^2$. For each bin the acceptance correction is applied and the contribution of the BH process is subtracted together with the estimated π^0 contamination. The photon flux factor is applied on an event-by-event basis according to Eq. (7). In every of the four bins in $|t|$, the mean value of the cross section is obtained by averaging over Q^2 and ν. When determining the cross section in bins of ϕ, no significant dependence on ϕ is observed. According to Eq. (5), the extracted result is in such a case sensitive to the quantity c_0^{DVCS} only.

4. Results

The t-dependence of the extracted μ^+ and μ^- cross section average is shown in Fig. 4, with the numerical values given in Table 1. The observed t-dependence of the DVCS cross section can

Table 2
Columns 1 and 2 show the relative systematic uncertainties on the measured cross section in bins of $|t|$, columns 3 and 4 show those on the fitted slope of the cross section. All values are given in percent. Note that the uni-directional systematic uncertainty $\sigma_\uparrow$ ($\sigma_\downarrow$) has to be used with positive (negative) sign.

Source	$\sigma_\uparrow^t$	$\sigma_\downarrow^t$	$\sigma_\uparrow^B$	$\sigma_\downarrow^B$
muon flux	3	3		
kinematic fit	3	3	0	0
background stat. unc.	2 - 5	2 - 5	2	2
background norm.	0	6 - 12	0	5
radiative corr.	0	4 - 6	0	1
reconstr. unc.	13 - 19	9	0	2
Σ	15 - 23	11 - 12	2	6

be well described by a single-exponential function $e^{-B|t|}$. The four data points are fitted using a binned maximum-likelihood method, where the weights take into account all corrections mentioned above. The result on the t-slope,

$$B = (4.3 \pm 0.6_{\text{stat}} {}^{+0.1}_{-0.3}\big|_{\text{sys}}) \ (\text{GeV}/c)^{-2}, \tag{9}$$

is obtained at the average kinematics $\langle W \rangle = 5.8 \ \text{GeV}/c^2$, $\langle Q^2 \rangle = 1.8 \ (\text{GeV}/c)^2$ and $\langle x_{\text{Bj}} \rangle = 0.056$.

In Table 2, the important contributions to the systematic uncertainties on the values of cross sections and exponential slope are shown, arranged in three groups. The first group contains symmetric contributions due to uncertainties in the determination of the beam flux, possible variations of the energy and momentum balance in the kinematic fit and the statistical uncertainty of the background subtraction. The second group contains systematic uncertainties related to corrections that were applied to the measured cross section. The subtracted amount of π^0 background is translated into an uni-directional systematic uncertainty of up to $+12\%$, which is related to the detection of photons and originates from a possible bias on the low energy-thresholds of the electromagnetic calorimeters. As radiative corrections to the DVCS process are model dependent, they are not applied but instead also included as an uni-directional systematic uncertainty. The third group contains the largest contribution to the systematic uncertainty. It is linked to the normalisation of the data in the large ν-range with respect to the Bethe-Heitler contribution, when comparing data taking with positively and negatively charged muon beam. It is asymmetric and amounts to at most $+19\%$ and -9% for large values of $|t|$. The total systematic uncertainty Σ is obtained as quadratic sum of all components shown in Table 2.

The main systematic uncertainty on the slope B is uni-directional with a value of -5% and originates from the normalisation of the π^0 background. Note that the systematic uncertainties of the four data points for the cross section are strongly correlated, so that for the slope value a considerably smaller systematic uncertainty is obtained. More details on systematic uncertainties are given in Ref. [23].

5. Interpretation

This Letter presents the first measurement of the $|t|$-dependence of the differential DVCS cross section in the intermediate x_{Bj}-region, which can be described by a single-exponential function $e^{-B|t|}$. Using Eq. (1), the fitted slope B of the measured $|t|$-dependence of the DVCS cross section is converted into the transverse extension of partons in the proton, as probed by DVCS at about $\langle x_{\text{Bj}} \rangle / 2 = 0.028$:
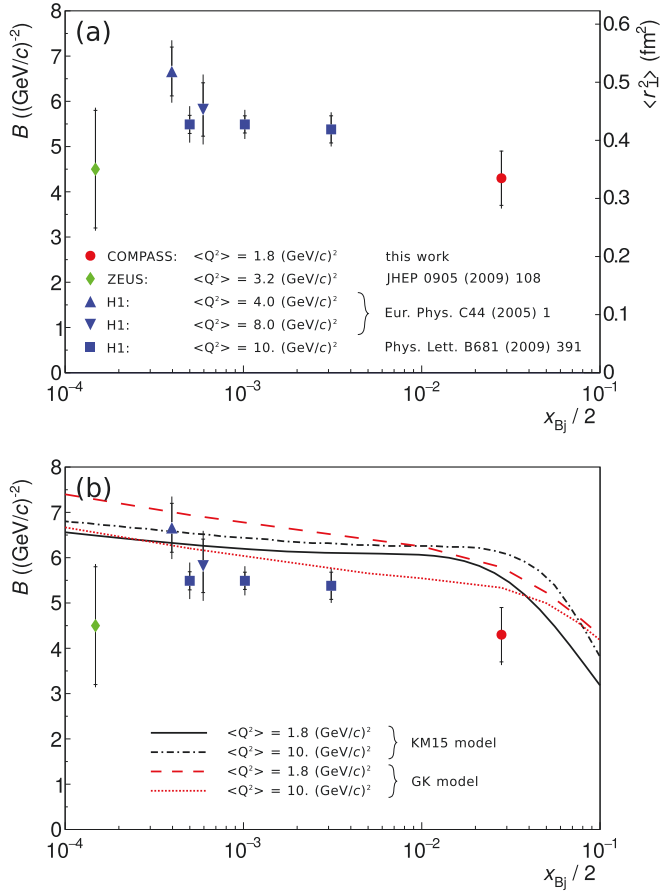
Fig. 5. (a) Results from COMPASS and previous measurements by H1 [26,27] and ZEUS [28] on the t-slope parameter B, or equivalently the average squared transverse extension of partons in the proton, $\langle r_\perp^2 \rangle$, as probed by DVCS at the proton longitudinal momentum fraction $x_{Bj}/2$ (see text). Inner error bars represent statistical and outer ones the quadratic sum of statistical and systematic uncertainties. (b) Same results compared to the predictions of the GK [29–31] and KM15 [32,33] models.

$$\sqrt{\langle r_\perp^2 \rangle} = (0.58 \pm 0.04_{\text{stat}} {}^{+0.01}_{-0.02}\big|_{\text{sys}} \pm 0.04_{\text{model}})\,\text{fm}. \tag{10}$$

The determination of the model uncertainty is explained below. Fig. 5 (a) shows our result together with those obtained by earlier high-energy experiments that used the same method to determine the DVCS cross section and extract the t-slope parameter B, or equivalently the average squared transverse extension of partons in the proton, $\langle r_\perp^2 \rangle$. We note that the results of the HERA collider experiments H1 [26,27] and ZEUS [28] were obtained at higher values of Q^2 as compared to that of the COMPASS measurement. Also, while our measurement probes the transverse extension of partons in the proton in the intermediate x_{Bj} range, the measurements at HERA are sensitive to values of $x_{Bj}/2$ below 10^{-2}.

As described e.g. in Ref. [13], the slope B of the $|t|$-dependence of the DVCS cross section can be converted into the transverse extension of partons in the proton assuming i) the dominance of the imaginary part of the CFF $\mathcal{H}$, and ii) a negligible effect of a non-zero value of the skewness $\xi \approx x_{Bj}/2$ in the actual measurement. Both assumptions are expected to hold at small values of x_{Bj}.

In the following, we interpret our measurement of the B-slope at leading order in α_S and at leading twist. In such a case, the spin-independent DVCS cross section is only sensitive to the quantity c_0^{DVCS} that is related at small x_{Bj} to the CFFs $\mathcal{H}$, $\tilde{\mathcal{H}}$ and $\mathcal{E}$ as [14]:

$$c_0^{DVCS} \propto 4(\mathcal{H}\mathcal{H}^* + \tilde{\mathcal{H}}\tilde{\mathcal{H}}^*) + \frac{t}{M^2}\mathcal{E}\mathcal{E}^*. \tag{11}$$

In the x_{Bj}-domain of COMPASS, c_0^{DVCS} is dominated by the imaginary part of the CFF $\mathcal{H}$. In this region, the contributions by the real part of $\mathcal{H}$ and by other CFFs amount to about 3% when calculated using the GK model [29–31] ported to the PARTONS framework [34] and to about 6% when using the KM15 model [32,33]. Using the second value, the systematic model uncertainty related to assumption i) above is estimated to be about ± 0.03 fm.

The skewness ξ is equal to one half of the longitudinal momentum fraction transferred between the initial and final proton. A strict relation between the slope B and $\langle r_\perp^2 \rangle$ only exists for $\xi = 0$. A non-zero value of ξ introduces an additional uncertainty on $\langle r_\perp^2 \rangle$ that is related to a shift of the centre of the reference system, in which $\langle r_\perp^2 \rangle$ is defined [8]. Using the GK model, we estimate the corresponding systematic uncertainty regarding assumption ii) above to be about ± 0.02 fm. The value for the model uncertainty given in Eq. (10) is obtained by quadratic summation of the two components.

The same data as presented in Fig. 5 (a) are shown in Fig. 5 (b), compared to calculations of the phenomenological GK and KM15 models, which describe the data reasonably well in the low and medium x_{Bj} range. Even taking into account the relatively small effect of Q^2 evolution, some scale offset between data and models seems to exist. When comparing our result on the transverse extension of partons in the proton to the lowest-Q^2 result of H1, there is an indication for shrinkage, i.e. a decrease of the B-slope with x_{Bj}, at the level of about 2.5 standard deviations of the combined uncertainty.

In order to reliably determine the full x_{Bj}-dependence of the transverse extension of partons in the proton, a global phenomenological analysis using all results from DVCS experiments at HERA, CERN, and JLab appears necessary to pin down the imaginary part of CFF $\mathcal{H}$, and eventually the GPD H itself. At leading order in α_s and at leading twist, such analyses [35,33,36–38,13] have already been performed in order to interpret the results of those experiments that access the high-x_{Bj} region, i.e. mostly the valence-quark sector probed by HERMES and at JLab (see e.g. Ref. [13] for a list of experimental results). In such a global analysis, the Q^2 evolution and all necessary corrections have to be included that are required under the kinematic conditions of the respective experiments. Possibly, also results on exclusive-meson production may be included. Eventually, this may allow one to disentangle the contributions of the different parton species to the transverse size of the proton as a function of the average longitudinal momentum fraction carried by its constituents.

6. Summary

In summary, using exclusive single-photon muoproduction we have measured the t-slope of the deeply virtual Compton scattering cross section at $\langle W \rangle = 5.8$ (GeV/c)^2, $\langle Q^2 \rangle = 1.8$ (GeV/c)^2 and $\langle x_{Bj} \rangle = 0.056$, which leads to the slope value $B = (4.3 \pm 0.6_{\text{stat}} {}^{+0.1}_{-0.3}\big|_{\text{sys}})$ (GeV/c)$^{-2}$. For an average longitudinal momentum fraction carried by the partons in the proton of about $\langle x_{Bj} \rangle/2 = 0.028$, we find a transverse extension of partons in the proton of $\sqrt{\langle r_\perp^2 \rangle} = (0.58 \pm 0.04_{\text{stat}} {}^{+0.01}_{-0.02}\big|_{\text{sys}} \pm 0.04_{\text{model}})\,\text{fm}$.

Acknowledgements

muon mass, Sergey Goloskokov and Peter Kroll for their continuous support with model predictions for the π^0 background extraction, as well as Kresimir Kumericki and Dieter Mueller for providing their theoretical predictions on the t-slope parameter B.

References

[1] D. Müller, D. Robaschik, B. Geyer, F.-M. Dittes, J. Hořejši, Fortschr. Phys. 42 (1994) 101.
[2] X.-D. Ji, Phys. Rev. Lett. 78 (1997) 610.
[3] X.-D. Ji, Phys. Rev. D 55 (1997) 7114.
[4] A.V. Radyushkin, Phys. Lett. B 380 (1996) 417.
[5] A.V. Radyushkin, Phys. Rev. D 56 (1997) 5524.
[6] M. Burkardt, Phys. Rev. D 62 (2000) 071503, Phys. Rev. D 66 (2002), 119903(i).
[7] M. Burkardt, Int. J. Mod. Phys. A 18 (2003) 173.
[8] M. Diehl, Eur. Phys. J. C 25 (2002) 223, Eur. Phys. J. C 31 (2003), 277(i).
[9] J.P. Ralston, B. Pire, Phys. Rev. D 66 (2002) 111501.
[10] N. d'Hose, S. Niccolai, A. Rostomyan, Eur. Phys. J. A 52 (2016) 151.
[11] L. Frankfurt, M. Strikman, C. Weiss, Annu. Rev. Nucl. Part. Sci. 55 (2005) 403.
[12] E.-C. Aschenauer, S. Fazio, K. Kumericki, D. Mueller, J. High Energy Phys. 09 (2013) 93.
[13] H. Moutarde, P. Sznajder, J. Wagner, Eur. Phys. J. C 78 (2018) 890.
[14] A.V. Belitsky, D. Müller, A. Kirchner, Nucl. Phys. B 629 (2002) 323.
[15] L.N. Hand, Phys. Rev. 129 (1963) 1834.
[16] P. Abbon, et al., COMPASS Collaboration, Nucl. Instrum. Methods A 577 (2007) 455.
[17] P. Abbon, et al., COMPASS Collaboration, Nucl. Instrum. Methods A 779 (2015) 69.
[18] F. Gautheron, et al., COMPASS Collaboration, SPSC-P-340, CERN-SPSC-2010-014.
[19] A. Sandacz, P. Sznajder, arXiv:1207.0333 [hep-ph].
[20] C. Regali, PhD thesis, University of Freiburg, 2016, https://doi.org/10.6094/UNIFR/11449;
T. Szameitat, PhD thesis, University of Freiburg, 2017, https://doi.org/10.6094/UNIFR/11686.
[21] L.L. Frankfurt, A. Freund, M. Strikman, Phys. Rev. D 58 (1998) 114001, Phys. Rev. D 59 (1999) 119901.
[22] L.L. Frankfurt, A. Freund, M. Strikman, Phys. Lett. B 460 (1999) 417.
[23] P. Jörg, PhD thesis, University of Freiburg, 2017, https://doi.org/10.6094/UNIFR/12397;
Exploring the Size of the Proton, Springer International Publishing, 2018.
[24] S.V. Goloskokov, P. Kroll, Eur. Phys. J. A 47 (2011) 112.
[25] C. Adolph, et al., COMPASS Collaboration, Phys. Lett. B 718 (2013) 922.
[26] A. Aktas, et al., H1 Collaboration, Eur. Phys. J. C 44 (2005) 1.
[27] F.D. Aaron, et al., H1 Collaboration, Phys. Lett. B 681 (2009) 391.
[28] S. Chekanov, et al., ZEUS Collaboration, J. High Energy Phys. 05 (2009) 108.
[29] S.V. Goloskokov, P. Kroll, Eur. Phys. J. C 42 (2005) 281.
[30] S.V. Goloskokov, P. Kroll, Eur. Phys. J. C 53 (2008) 367.
[31] S.V. Goloskokov, P. Kroll, Eur. Phys. J. C 65 (2010) 137.
[32] K. Kumericki, D. Müller, Nucl. Phys. B 841 (2010) 1.
[33] K. Kumericki, D. Müller, EPJ Web Conf. 112 (2016) 01012.
[34] B. Berthou, et al., Eur. Phys. J. C 78 (2018) 478.
[35] K. Kumericki, D. Müller, M. Murray, Phys. Part. Nucl. 45 (2014) 723.
[36] K. Kumericki, S. Liuti, H. Moutarde, Eur. Phys. J. A 52 (2016) 157.
[37] R. Dupre, M. Guidal, M. Vanderhaeghen, Phys. Rev. D 95 (2017) 011501.
[38] R. Dupré, M. Guidal, S. Niccolai, M. Vanderhaeghen, Eur. Phys. J. A 53 (2017) 171.

The COMPASS Collaboration

R. Akhunzyanov [g], M.G. Alexeev [y], G.D. Alexeev [g], A. Amoroso [y,z], V. Andrieux [ab,t], N.V. Anfimov [g], V. Anosov [g], A. Antoshkin [g], K. Augsten [g,r], W. Augustyniak [ac], A. Austregesilo [o], C.D.R. Azevedo [a], B. Badełek [ad], F. Balestra [y,z], M. Ball [c], J. Barth [d], R. Beck [c], Y. Bedfer [t], J. Bernhard [l,i], K. Bicker [o,i], E.R. Bielert [i], R. Birsa [x], M. Bodlak [q], P. Bordalo [k,1], F. Bradamante [w,x], A. Bressan [w,x], M. Büchele [h], E. Burtin [t], V.E. Burtsev [aa], W.-C. Chang [u], C. Chatterjee [f], M. Chiosso [y,z], I. Choi [ab], A.G. Chumakov [aa], S.-U. Chung [o,2], A. Cicuttin [x,3], M.L. Crespo [x,3], S. Dalla Torre [x], S.S. Dasgupta [f], S. Dasgupta [w,x], O.Yu. Denisov [z,*], L. Dhara [f], S.V. Donskov [s], N. Doshita [af], Ch. Dreisbach [o], W. Dünnweber [4], R.R. Dusaev [aa], M. Dziewiecki [ae], A. Efremov [g,5], P.D. Eversheim [c], A. Ferrero [t,*], M. Finger [q], M. Finger jr. [q], H. Fischer [h], C. Franco [k], N. du Fresne von Hohenesche [l,i], J.M. Friedrich [o,*], V. Frolov [g,i], E. Fuchey [t,6,7], F. Gautheron [b,ab], O.P. Gavrichtchouk [g], S. Gerassimov [n,o], J. Giarra [l], I. Gnesi [y,z], M. Gorzellik [h,8], A. Grasso [y,z], A. Gridin [g], M. Grosse Perdekamp [ab], B. Grube [o], T. Grussenmeyer [h], A. Guskov [g], D. Hahne [d], G. Hamar [x], D. von Harrach [l], R. Heitz [ab], F. Herrmann [h], N. Horikawa [p,9], N. d'Hose [t], C.-Y. Hsieh [u,10], S. Huber [o], S. Ishimoto [af,11], A. Ivanov [y,z], Yu. Ivanshin [g], T. Iwata [af], V. Jary [r], R. Joosten [c], P. Jörg [h,12,*], K. Juraskova [r], E. Kabuß [l], A. Kerbizi [w,x], B. Ketzer [c], G.V. Khaustov [s], Yu.A. Khokhlov [s,13], Yu. Kisselev [g], F. Klein [d], J.H. Koivuniemi [b,ab], V.N. Kolosov [s], K. Kondo [af], I. Konorov [n,o], V.F. Konstantinov [s], A.M. Kotzinian [z,14], O.M. Kouznetsov [g], Z. Kral [r], M. Krämer [o], F. Krinner [o], Z.V. Kroumchtein [g,31], Y. Kulinich [ab], F. Kunne [t], K. Kurek [ac], R.P. Kurjata [ae], I.I. Kuznetsov [aa], A. Kveton [r], A.A. Lednev [s,31], E.A. Levchenko [aa], M. Levillain [t], S. Levorato [x], Y.-S. Lian [u,15], J. Lichtenstadt [v], R. Longo [y,z], V.E. Lyubovitskij [aa,16], A. Maggiora [z], A. Magnon [ab], N. Makins [ab], N. Makke [x,3], G.K. Mallot [i], S.A. Mamon [aa], B. Marianski [ac], A. Martin [w,x], J. Marzec [ae], J. Matoušek [w,x,q], H. Matsuda [af], T. Matsuda [m], G.V. Meshcheryakov [g], M. Meyer [ab,t], W. Meyer [b], Yu.V. Mikhailov [s], M. Mikhasenko [c], E. Mitrofanov [g], N. Mitrofanov [g], Y. Miyachi [af], A. Moretti [w], A. Nagaytsev [g], F. Nerling [l], D. Neyret [t], J. Nový [r,i], W.-D. Nowak [l], G. Nukazuka [af], A.S. Nunes [k], A.G. Olshevsky [g], I. Orlov [g], M. Ostrick [l], D. Panzieri [z,17], B. Parsamyan [y,z], S. Paul [o], J.-C. Peng [ab], F. Pereira [a], M. Pešek [q], M. Pešková [q], D.V. Peshekhonov [g], N. Pierre [l,t], S. Platchkov [t], J. Pochodzalla [l], V.A. Polyakov [s], J. Pretz [d,18], M. Quaresma [k], C. Quintans [k], S. Ramos [k,1], C. Regali [h], G. Reicherz [b], C. Riedl [ab], N.S. Rogacheva [g], D.I. Ryabchikov [s,o], A. Rybnikov [g], A. Rychter [ae], R. Salac [r], V.D. Samoylenko [s], A. Sandacz [ac], C. Santos [x], S. Sarkar [f], I.A. Savin [g,5], T. Sawada [u], G. Sbrizzai [w,x], P. Schiavon [w,x], H. Schmieden [d], K. Schönning [i,19], E. Seder [t], A. Selyunin [g], L. Silva [k], L. Sinha [f], S. Sirtl [h], M. Slunecka [g], J. Smolik [g], A. Srnka [e], D. Steffen [i,o], M. Stolarski [k], O. Subrt [i,r], M. Sulc [j], H. Suzuki [af,9], A. Szabelski [w,x,ac], T. Szameitat [h,8], P. Sznajder [ac], M. Tasevsky [g], S. Tessaro [x], F. Tessarotto [x],

A. Thiel [c], J. Tomsa [q], F. Tosello [z], V. Tskhay [n], S. Uhl [o], B.I. Vasilishin [aa], A. Vauth [i], B.M. Veit [l], J. Veloso [a],
A. Vidon [t], M. Virius [r], S. Wallner [o], M. Wilfert [l], J. ter Wolbeek [h,8], K. Zaremba [ae], P. Zavada [g],
M. Zavertyaev [n], E. Zemlyanichkina [g,5], N. Zhuravlev [g], M. Ziembicki [ae]

[a] *University of Aveiro, Dept. of Physics, 3810-193 Aveiro, Portugal*
[b] *Universität Bochum, Institut für Experimentalphysik, 44780 Bochum, Germany* [20,21]
[c] *Universität Bonn, Helmholtz-Institut für Strahlen- und Kernphysik, 53115 Bonn, Germany* [20]
[d] *Universität Bonn, Physikalisches Institut, 53115 Bonn, Germany* [20]
[e] *Institute of Scientific Instruments, AS CR, 61264 Brno, Czech Republic* [22]
[f] *Matrivani Institute of Experimental Research & Education, Calcutta-700 030, India* [23]
[g] *Joint Institute for Nuclear Research, 141980 Dubna, Moscow region, Russia* [5]
[h] *Universität Freiburg, Physikalisches Institut, 79104 Freiburg, Germany* [20,21]
[i] *CERN, 1211 Geneva 23, Switzerland*
[j] *Technical University in Liberec, 46117 Liberec, Czech Republic* [22]
[k] *LIP, 1000-149 Lisbon, Portugal* [24]
[l] *Universität Mainz, Institut für Kernphysik, 55099 Mainz, Germany* [20]
[m] *University of Miyazaki, Miyazaki 889-2192, Japan* [25]
[n] *Lebedev Physical Institute, 119991 Moscow, Russia*
[o] *Technische Universität München, Physik Dept., 85748 Garching, Germany* [20,4]
[p] *Nagoya University, 464 Nagoya, Japan* [25]
[q] *Charles University in Prague, Faculty of Mathematics and Physics, 18000 Prague, Czech Republic* [22]
[r] *Czech Technical University in Prague, 16636 Prague, Czech Republic* [22]
[s] *State Scientific Center Institute for High Energy Physics of National Research Center 'Kurchatov Institute', 142281 Protvino, Russia*
[t] *IRFU, CEA, Université Paris-Saclay, 91191 Gif-sur-Yvette, France* [21]
[u] *Academia Sinica, Institute of Physics, Taipei 11529, Taiwan* [26]
[v] *Tel Aviv University, School of Physics and Astronomy, 69978 Tel Aviv, Israel* [27]
[w] *University of Trieste, Dept. of Physics, 34127 Trieste, Italy*
[x] *Trieste Section of INFN, 34127 Trieste, Italy*
[y] *University of Turin, Dept. of Physics, 10125 Turin, Italy*
[z] *Torino Section of INFN, 10125 Turin, Italy*
[aa] *Tomsk Polytechnic University, 634050 Tomsk, Russia* [28]
[ab] *University of Illinois at Urbana-Champaign, Dept. of Physics, Urbana, IL 61801-3080, USA* [29]
[ac] *National Centre for Nuclear Research, 00-681 Warsaw, Poland* [30]
[ad] *University of Warsaw, Faculty of Physics, 02-093 Warsaw, Poland* [30]
[ae] *Warsaw University of Technology, Institute of Radioelectronics, 00-665 Warsaw, Poland* [30]
[af] *Yamagata University, Yamagata 992-8510, Japan* [25]